Design of a Movable Nested-Mesh Primitive Equation Model

YOSHIO KURIHARA, GREGORY J. TRIPOLI[1] AND MORRIS A. BENDER

Geophysical Fluid Dynamics Laboratory/NOAA, Princeton University, Princeton, NJ 08540

(Manuscript received 21 August 1978, in final form 28 November 1978)

ABSTRACT

A numerical scheme to construct a two-way, movable, nested-mesh primitive equation model is proposed. Dynamical coupling in a two-way nesting system is performed at a dynamical interface which is separated from a mesh interface by two coarse-grid intervals. Dynamical interaction is achieved by a method which conserves mass, momentum and internal energy of the system. During the course of integration, the nested mesh moves so that the central position of the disturbance contained in the fine-mesh area never deviates from the center of the nest by more than one coarse-mesh interval. New grid data near the leading and trailing edges of the moving nest are obtained by an interpolation method which has a conservation property. The proposed methods of dynamical coupling and mesh movement were extensively tested by a one-dimensional shallow water equation model. Numerical results of these experiments are presented.

1. Introduction

The purpose of this paper is to describe a basic numerical scheme of a movable nested-mesh primitive equation model. The scheme has been utilized in a tropical cyclone model at the Geophysical Fluid Dynamics Laboratory, NOAA. The proposed methods were tested extensively with a one-dimensional shallow water equation model before being incorporated into a three-dimensional model. These test results are presented in order to demonstrate the performance of the scheme.

The nested-mesh system considered in this study belongs to a class of two-way nesting systems. In a two-way system, the time integration proceeds simultaneously for a fine and a coarse resolution mesh area so that the two mesh areas interact dynamically with each other. This differs from a one-way approach in which a time integration is performed first for the total domain by using a coarse resolution and then the integration is redone for an inner limited area by utilizing a fine resolution. The boundary conditions for the latter integration are derived from the earlier one. A list of works previously done along this line may be found in a paper by Miyakoda and Rosati (1977). Depending on the nature of the problems, one may choose either a one-way or two-way system to treat the evolution of small-scale disturbances in a larger scale environment. So far, two-way nesting systems have been adopted in some numerical modeling studies of tropical cyclones. Such past attempts are specifically mentioned in a paper by Ley and Elsberry (1976).

In a two-way nesting system, dynamical interaction between the two neighboring domains can be achieved in various ways. A fairly common technique is to transfer meteorological information from a fine to a coarse mesh and vice versa frequently at a narrow zone where the two meshes overlap (e.g., Harrison and Elsberry, 1972; Phillips and Shukla, 1973). Two non-overlapping adjacent meshes may be dynamically coupled when the time integration for the grid points near the mesh interface is performed in each side with the use of the information in the other mesh domain (Ookochi, 1972). This idea was useful in developing nesting tactics for the present work. One of the original features of the nesting scheme proposed in this paper is that an interface where the two integration domains interact with each other (dynamical interface) is intentionally separated from the mesh interface. This is done in order to keep possible numerical shock due to a dynamical coupling from occurring at the mesh interface where noise may also result from the change in grid resolution. Furthermore, the interaction at the dynamical interface is expressed in the form of a flux condition so that the transports of mass, momentum and internal energy do not yield fictitious increases nor decreases of these quantities. The finite difference scheme used in this study reduces exactly to an ordinary "box" method (Kurihara and Holloway, 1967) if the resolutions of all meshes become the same.

In Section 2 the grid structure of the proposed nested system is defined and the treatment of the

[1] Present affiliation: Department of Atmospheric Science, Colorado State University, Fort Collins, 80521.

dynamical interaction between two integration domains is described. Section 3 deals with a scheme for moving a nested fine mesh within a coarse mesh. In Section 4 numerical examples are presented to demonstrate the performance of the proposed two-way nesting system.

2. A two-way nesting system

a. Mesh structure

The configuration of mesh nesting in the present study is simple. Fig. 1 shows the mesh structures for a one-dimensional and a two-dimensional (longitude-latitude) domain, respectively. Each mesh, except for the innermost one, encloses a finer resolution mesh. Since there is no overlapping of meshes, the interface between the two adjacent meshes is clearly defined. Hereafter, two meshes of different resolution joining at any interface will be respectively referred to as a coarse mesh (CM) and a fine mesh (FM). Grid spacing of a coarse mesh is defined as a multiple of that of a fine mesh. (In the GFDL nested-mesh model, the number of meshes, the grid spacing ratios between two adjacent meshes and the area of each mesh domain are all disposable parameters.) In Fig. 1, the dots indicate the grid points which are placed at the center of each box, i.e., a mesh element. Grid points are not staggered and all meteorological variables are defined at the same point.

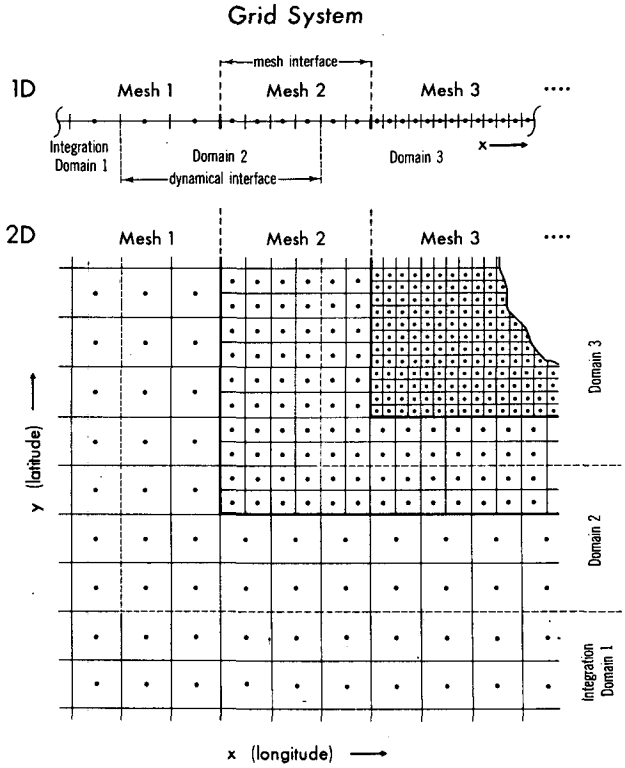

FIG. 1. Configuration of grids (dots) in one-dimensional (upper part) and two-dimensional (lower part) domains.

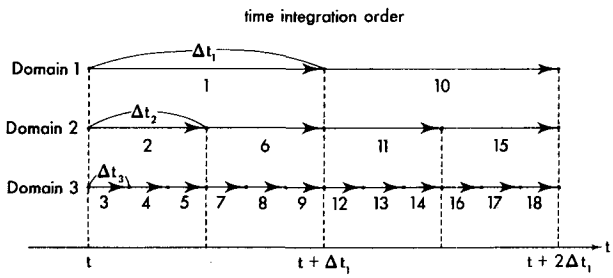

FIG. 2. Time integration order for the case of a triple integration domain.

The time integration of a nested mesh model is usually performed with different time increments for each integration domain. In the present study, the integration domains are bounded by the dynamical interfaces which are intentionally separated from the mesh interfaces by two coarse-grid intervals as shown in Fig. 1. Accordingly, the integration for the inner two grid points of CM are made when FM is integrated.

b. Time integration method

The rules defining the order of time integration in the present model are as follows: 1) the integration of a certain integration domain proceeds only when all the inner domains are integrated up to the time-level of that domain, and 2) when two or more integration domains are synchronized, the integration proceeds from the outermost domain of those synchronized to the inner domains. An example of the time integration order is schematically presented in Fig. 2 for the case of a triple integration domain.

The time integration may be performed by a scheme proposed by Kurihara and Tripoli (1976) which is designed to preserve low-frequency waves in a primitive equation model while suppressing high-frequency noises. A local tendency of a quantity h may be expressed as

$$\frac{\partial h}{\partial t} = \mathrm{LF} + \mathrm{HF} + \mathrm{DIF}, \qquad (2.1)$$

where t is time and the right-hand side consists of the advection terms which usually yield a low frequency change (LF), the terms primarily relating to high frequency mode (HF) and the diffusion terms (DIF). The numerical integration of (2.1) may be made by the following two-step iterative scheme:

$$\left.\begin{aligned} (h^* - h^\tau)/\Delta t &= \mathrm{LF}^\tau + \mathrm{HF}^\tau + \mathrm{DIF} \\ (h^{\tau+1} - h^\tau)/\Delta t &= [(1-\alpha)\cdot\mathrm{LF}^\tau + \alpha\cdot\mathrm{LF}^*] \\ &\quad + [(1-\beta)\cdot\mathrm{HF}^\tau + \beta\cdot\mathrm{HF}^*] + \mathrm{DIF} \end{aligned}\right\}. \qquad (2.2)$$

In (2.2), τ and $\tau+1$ are time levels, Δt a time increment, h^* a temporary value, and the superscripts attached to the terms indicate the time level for which those terms are calculated. The diffusion term may be estimated either explicitly at the time level τ (the horizontal diffusion term in the present model) or implicitly (the vertical diffusion term). In the present study, the weights α and β in (2.2) were chosen to be 0.506 and 1, respectively. The terms other than the advection and diffusion terms were treated as the HF. If another term such as the effect of diabatic heating is included in the right hand side of (2.1), then the change due to this effect may be added after the iteration (2.2) is performed.

When the σ-coordinate system (see Phillips, 1957) is used in modeling, the equation for a quantity h often takes the form

$$\frac{\partial(hp_*)}{\partial t} = -D(h) + \ldots,$$

where p_* is the surface pressure and, $D(h)$ denotes the sum of the horizontal divergence $\nabla\cdot(hp_*\mathbf{v})$ and the vertical flux divergence $\partial(hp_*\dot{\sigma})/\partial\sigma$ (see Kurihara and Holloway, 1967). The above equation may be rewritten as

$$\frac{\partial(hp_*)}{\partial t} = -D(h) + hD(1) - hD(1) + \ldots, \quad (2.3)$$

where $D(1)$ means the mass divergence $\nabla\cdot(p_*\mathbf{v}) + \partial(p_*\dot{\sigma})/\partial\sigma$. The sum of the first two terms in the right hand side of (2.3) represents the advection $-p_*\mathbf{v}\cdot\nabla h - p_*\dot{\sigma}\partial h/\partial\sigma$. Therefore, these two terms correspond to the LF of (2.1). The third term in the right hand side of (2.3) should be included in the HF of (2.1).

c. *Dynamical interaction*

In the present two-way nesting system, a dynamical interface is defined at a distance of two coarse-grid intervals outward from the mesh boundary. A strategy for dynamic coupling of the two integration regions is illustrated in Fig. 3 for the case of a one-dimensional nest. In this figure, an area of interest near the mesh interface is shown at the top. The large dots symbolize the status of the grids at time t. The open circles denote the results of prediction for $t + \Delta t_c$ (Δt_c is a coarse time interval), while the cross marks are used to indicate the intermediate status at a smaller time interval Δt_f. As shown in the figure, a prognosis is made first for the area outside of the dynamical interface. The initial condition for this marching is given by data in the CM area only. In the course of integration, meteorological quantities and their fluxes at the dynamical interface are computed. These values are preserved for the use in prognosis 2 in which the

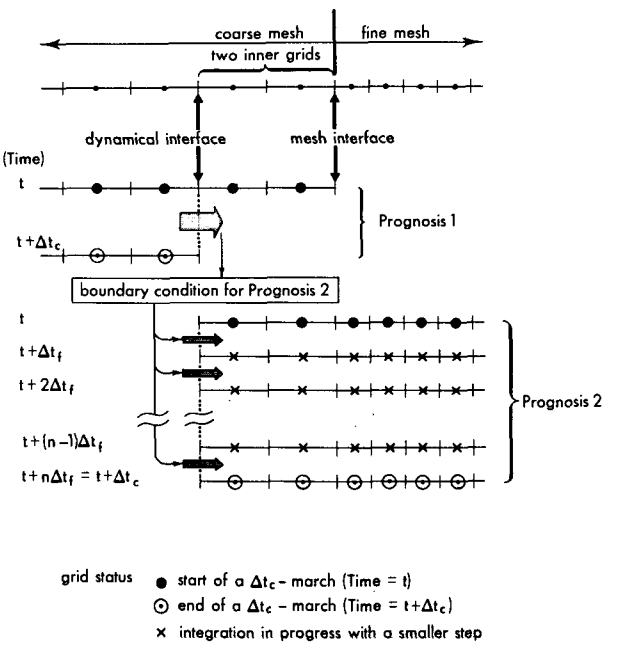

FIG. 3. Schematic chart showing a strategy of dynamic coupling of two integration domains.

integration is performed for the area inside of the dynamical interface, i.e., for the FM area plus two inner coarse grids. Usually, prognosis 2 consists of a few marchings of a smaller time step Δt_f. At each marching, the boundary conditions at the dynamical interface are derived from the values obtained at prognosis 1. If the conservation of a quantity is required, it can be satisfied by making the total flux of that quantity across the boundary during prognosis 2 equal to that during prognosis 1. The scheme of integration mentioned above establishes a two-way system, because the area outside of the dynamical interface is influenced by the inner area in prognosis 1, and the inner area is forced by the outer area in prognosis 2.

Using the same strategy as explained above, one can construct a two-way nesting system in a two-dimensional domain. Fig. 4 illustrates such a system. The line M in the figure separates the CM domain and the FM domain. The FM area, C, is surrounded by a narrow zone B. The outer rim of the zone, indicated by the line N, is the dynamical interface of this system. In prognosis 1, the prediction is made for area A with the use of data in areas A and B. Various meteorological information on the interface N during prognosis 1 is preserved. This information is utilized in prognosis 2 to specify the boundary condition along the line N in order to make the prediction for the area B plus C.

Next, a scheme for the time interpolation of boundary conditions in prognosis 2 is considered. Suppose that an equation which is written in the flux form (2.3) is integrated with (2.2). Denoting the

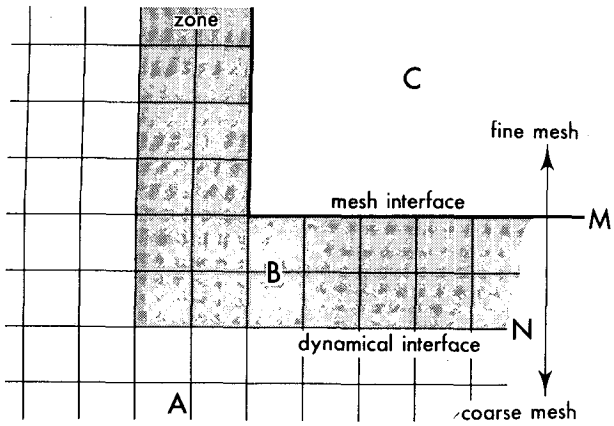

FIG. 4. In a two-dimensional domain, a dynamical interface (line N) is separated from a mesh interface (line M) by a narrow zone B (shaded).

normal flux of a quantity across the dynamical interface at the time levels τ and $*$ (temporary advanced level) in prognosis 1 by F^0 and F^1, respectively, one obtains the flux in the corrector step from $[(1-\alpha)F^0 + \alpha F^1]$. Similarly, the flux in a short marching step in prognosis 2 may be given by $[(1-\alpha)f_m^0 + \alpha f_m^1]$, where f is the flux in a short step and m represents the step number which proceeds from 1 to n ($n = \Delta t_c/\Delta t_f$). The condition of conservation may be expressed by

$$[(1-\alpha)F^0 + \alpha F^1]\Delta t_c = \sum_{m=1}^{n} [(1-\alpha)f_m^0 + \alpha f_m^1]\Delta t_f. \quad (2.4)$$

Since F^1 is taken for the flux at the advanced time level, it is desirable that (2.4) is satisfied while f_m^1 smoothly approaches F^1 as m increases. This is met when f_m^0 and f_m^1 are computed by

$$\left.\begin{aligned} f_m^0 &= \frac{n-m+1}{n}F^0 + \frac{m-1}{n}F^1 \\ f_m^1 &= \frac{n-m}{n}\left\{F^0 + \frac{2\alpha-1}{\alpha} \times (F^1 - F^0)\right\} + \frac{m}{n}F^1 \end{aligned}\right\}. \quad (2.5)$$

The above formulas show that f_m^0 is obtained from linear interpolation between F^0 and F^1, while f_m^1 is computed by an interpolation which has reduced weight on F^0 (if $\alpha > 0.5$). Note that f_m^1 in (2.5) reduces to F^1 if $\alpha = 1$. In the present modeling work, fluxes of momentum, temperature and mixing ratio across the dynamical interface during prognosis 2 are obtained from (2.5). Accordingly, the conservations of momentum, internal energy and latent energy are exact. On the other hand, the wind and the mass flux at the interface during prognosis 2 are specified by the following formulas, which correspond to (2.5) with $\alpha = 0.5$:

$$\left.\begin{aligned} f_m^0 &= \frac{n-m+1}{n}F^0 + \frac{m-1}{n}F^1 \\ f_m^1 &= \frac{n-m}{n}F^0 + \frac{m}{n}F^1 \end{aligned}\right\}. \quad (2.6)$$

The reason for the use of (2.6) is that it yields a gradual change in f_m and hence smooth time variation in the vertical velocity and the surface pressure at a boundary box. Although the mass conservation is not exact unless $\alpha = 0.5$, it is practically perfect in the present study. The geopotential or the pressure at the dynamical interface is also required to compute the pressure gradient force. It is determined from the surface pressure and the temperature at the interface. A formula similar to (2.6) is used to obtain these quantities during prognosis 2.

d. Spatial finite differencing

The finite difference equations for the present nested mesh model are formulated based on the so-called box method, version 1 (Kurihara and Holloway, 1967), with some modifications. In the box method, the flux divergence of any quantity from a key box is estimated from the sum of fluxes across the interfaces between a key box and contiguous boxes. In the present work, quantities such as wind velocity, surface pressure and any advected quantity at an interface are obtained through linear interpolation of grid values rather than from simple average of grid values. The upper part of Fig. 5 shows how to obtain a value at a mesh interface in a two-dimensional nest. In this case, linear interpolation is made first in the direction parallel to an interface m to obtain values at the open circles between the coarse grids. Then, linear interpolation along a perpendicular to the line m is applied between the open circles and the fine grid points to estimate the values at the cross marks on the mesh interface. Compared with the original box method, the above scheme gives a more accurate value at the mesh interface and causes less noise in the course of time integration of a model. The conservation property of kinetic energy in the original box method does not hold exactly at the mesh interface. It is, however, still preserved in the interior of each mesh domain because of the regular configuration of grids.

In the box method, the gradient of a quantity is computed from a value at the center of a box and those on its sides. When a box faces more than one box along one side, an average value along that side is taken as a side value in the original box method. In the present scheme, a linearly inter-

polated value to the mid-point of a side is utilized. For example, in the case of the lower part of Fig. 5, the west–east gradient of a quantity A is obtained from $w_E(A_E - A_K) + w_W(A_K - A_W)$, where A_E and A_W are the linearly interpolated values between the CM grids and a weight w is equal to a side length divided by the area of a box. The south–north gradient is estimated by $w_N(A_N - A_K) + w_S(A_K - A_S)$. Linear interpolation between the two CM grids yields A_N, while interpolation between b and c on the line m gives A_S. The values at b and c are obtained in the manner described above. If the grid ratio between the CM and the FM is odd, A_S coincides with the northern side value of the middle fine box.

It is noted here that the abovementioned modifications are made in order to reduce a computational excitation of noise in a moving nested mesh model. The proposed method becomes identical to an energy-conserving box method if nested meshes are reduced to a single uniform mesh.

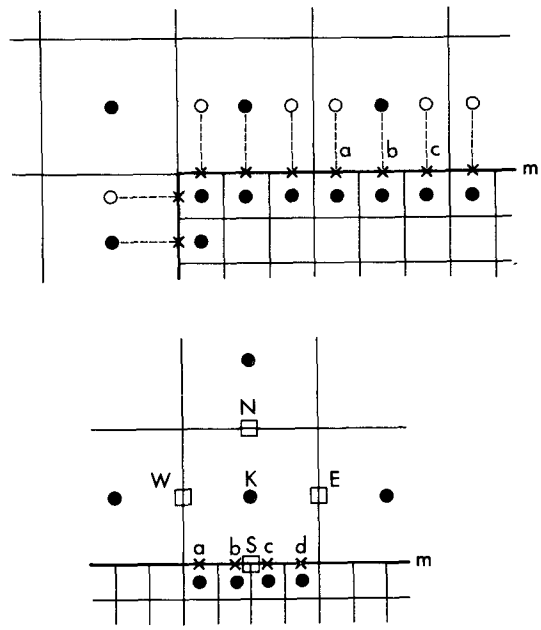

FIG. 5. Interpolation near a mesh interface m. Black dots indicate grid points. Values at the coarse grids are first interpolated to the auxiliary points (open circles). Subsequent interpolation between the auxiliary points and the fine grids yields the values at the interface points (cross marks). In the lower part, open squares indicate the north (N), east (E), south (S) and west (W) points for a key grid (K).

3. Movement of a nest

When a small-scale disturbance moves in the course of a time integration, it can be followed with a moving nested fine mesh. In the problem of mesh movement, the position of a disturbance has to be defined appropriately. A location of minimum surface pressure in a certain domain or the location of an apparent center of gravity of a given field may be used to determine such a position. Then, the position of the disturbance can be checked against the center of a certain mesh domain whenever that mesh is synchronized with the outer mesh. If the position difference in any coordinate direction exceeds a grid spacing of the outer coarse mesh, the mesh is shifted by a multiple, usually one, of the coarse grid distance so that the disturbance is relocated near the center of the mesh.

When a FM domain moves, a part of the CM domain becomes a new FM area and a part of the FM becomes a CM area. If the schemes to be presented below are used to establish new grid data in the affected areas, the area integral of a variable will remain unchanged after the mesh is moved. Accordingly, the conservation of mass, momentum and internal energy can be maintained.

If n FM boxes are combined to form a single CM box, a new value A_0 of a certain quantity is given by

$$A_0 = \sum_{i=1}^{n} (a_i \Delta s_i)/\Delta S_0, \tag{3.1}$$

where a_i is the value in a small FM box. A small box has the area Δs_i, and a large one has ΔS_0 which is equal to the sum of Δs_i. The conservation property is obvious in (3.1).

Next, suppose that one CM box has to be divided into n FM boxes in the longitude-latitude coordinate system. Denoting the longitude and latitude of a box center by λ_i and ϕ_i, respectively, and the radius of the earth by r and using the same notations as used in (3.1), one can specify a new value a_i for a new small box by

$$a_i = A_0 + \left(\frac{\partial A}{\alpha \partial \lambda}\right)_0 \alpha(\lambda_i - \lambda_0) + \left(\frac{\partial A}{r \partial \phi}\right)_0 \left(\frac{\Delta S_0}{n \Delta s_i}\right) r(\phi_i - \phi_0), \tag{3.2}$$

where $\alpha = r \cos\phi_0$ and the zonal and the meridional gradients are those evaluated for the CM field. The factor $\Delta S_0/(n\Delta s_i)$ is included in (3.2) so that the conservation condition is satisfied; i.e., $\Sigma a_i \Delta s_i = A_0 \Delta S_0$. {Note that $\Sigma(\lambda_i - \lambda_0)\ \Delta s_i = 0$ and $\Sigma[(\Delta S_0/n\Delta s_i)\ (\phi_i - \phi_0)\Delta s_i] = 0$.} It is easy to modify (3.1) and (3.2) to the formulas applicable to a one-dimensional mesh system.

There is no guarantee that the mass and wind fields are dynamically balanced with each other after the application of (3.1) or (3.2). Probably, inertia-gravity waves will be excited. It should be a serious concern whether the generated noise can be damped quickly by some means or not. However, an effective damping scheme has been devised which suppresses the noise caused by a mesh

movement in a nonlinear, three-dimensional, nested-mesh primitive equation model. This method will be explained in a paper appearing in the future.

4. Numerical tests

In this section, the capabilities of the present two-way nesting system are demonstrated by integration of a one-dimensional primitive equation model. This same model had been extensively used to investigate the various nesting techniques before the proposed strategy was established.

a. Test of dynamical interaction

We consider a wave train which propagates along a one-dimensional cyclic channel domain. Prediction of such a wave will be made by a nested mesh system fixed to the channel. If a two-way nesting method works satisfactorily, a wave train should move repeatedly from the CM domain into the FM domain and out again to the CM domain without causing any significant noise.

In this study, a perturbation is governed by the linearized shallow water equations;

$$\left.\begin{aligned} \frac{\partial u}{\partial t} &= -U\frac{\partial u}{\partial x} + fv - \frac{\partial \phi}{\partial x} \\ \frac{\partial v}{\partial t} &= -U\frac{\partial v}{\partial x} - fu \\ \frac{\partial \phi}{\partial t} &= -U\frac{\partial \phi}{\partial x} + fUv - gH\frac{\partial u}{\partial x} \end{aligned}\right\}, \quad (4.1)$$

where symbols are conventional. The constants are set to $U = 50$ m s^{-1}, f taken at 45° latitude and $gH = 8 \times 10^4$ m^{2}s^{-2}. Note that a strong basic flow is chosen so as to make the test condition severe. Solutions of (4.1) are described in Kurihara and Tripoli (1976). In this experiment, the initial fields are derived from the geopotential perturbation consisting of a slowly moving sinusoidal wave with the amplitude 1000 m^{2}s^{-2} and two inertia-gravitational waves with the amplitude 50 m^{2}s^{-2} each. Since those initial amplitudes are used regardless of the wavelength, the initial wind perturbation is larger for a wave with a smaller scale.

In Fig. 6, the initial fields of ϕ with wavelengths of 4200 km and 600 km are drawn in parts (a) and (c), respectively. At the top of (a), the domain sizes of the CM and the FM are shown. Dashed lines indicate the mesh interfaces. The grid distances of the CM and the FM are 60 and 30 km, respectively. The time increment for the two integration domains are 120 and 60 sec. A point P is fixed to each of the wave trains. Its initial position is P_0. The fields of ϕ and the positions of P after 48 h integration are presented in parts (b) and (d). At the bottom of each part, the change of x coordinate of the point P during the integration is indicated by the arrows. Both wave trains moved through the cyclic channel for a distance of almost two cycles. The initial shape of each wave is preserved well. Thus, in these cases, the proposed two-way nesting strategy worked. If a slow wave moves with an accurate speed and the inertia-gravity waves are damped by 48 h, the traced point should be found at the mark Q in parts (b) and (d) of the figure. It is seen that the phase speed of the computed wave is pretty accurate in the case of the 4200 km wave, but slightly less than the analytical value in the case of the 600 km wave.

Eq. (4.1) used for the above test does not include the diffusion terms. In the next experiments, the diffusion terms are added to (4.1) and integrations are performed to see whether these added terms cause any problem in a two-way system. At the dynamical interface, diffusive fluxes are computed at prognosis 1 and are subdivided equally into boundary diffusive fluxes at prognosis 2, so that there are no spurious sources of quantities at the interface. In a one-dimensional model, the diffusive flux of a quantity h between two adjacent boxes is obtained by $-K\,\partial h/\partial x$, where K is a diffusion coefficient. The coefficient expressing a nonlinear viscosity is

$$K = k_0\Delta^2\left[\left(\frac{\partial u}{\partial x}\right)^2 + \left(\frac{\partial v}{\partial x}\right)^2\right]^{1/2}. \quad (4.2)$$

In (4.2), k_0 is a parameter to be specified and Δ denotes the distance between the two grids. In case of a linear viscosity, the diffusion coefficient is given by

$$K = 0.2\Delta^{4/3}, \quad (4.3)$$

where both K and Δ are in cgs units. In any case, K is dependent on Δ. Accordingly, a test is needed concerning the effect of diffusion in a nested-mesh model.

Predictions of a wave train with a wavelength of 600 km were performed including the diffusion effects. The initial geopotential perturbation is the same as that in Fig. 6c. Geopotential fields after 48 h of integration are presented in Figs. 7a and 7b. Both nonlinear and linear viscosities reduced the amplitude of waves in the channel more or less uniformly. No numerical problems appeared at the mesh interfaces.

As mentioned before, the finite difference schemes used in the present study have some unique features. As to the space differencing, the original box method (Kurihara and Holloway, 1967) is modified so that a value at a box interface is evaluated from linear interpolation of grid values. The result of integration with the new method (Fig. 6d) may be compared against that obtained with the original box method (Fig. 7c). The improvement

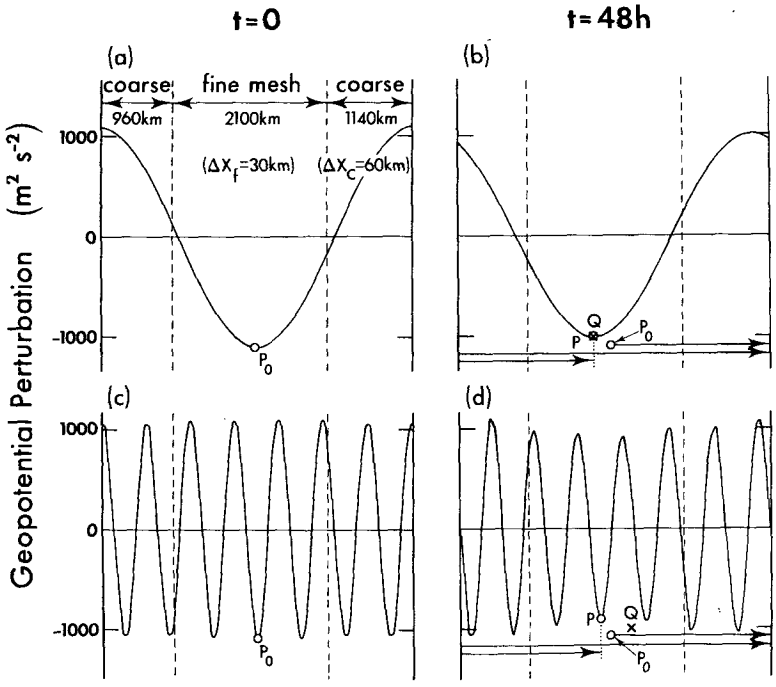

FIG. 6. Movement of wave trains through a nested mesh system in a one-dimensional cyclic free-surface channel. Geopotential perturbations of 4200 km wave (upper) and 600 km wave (lower) at $t = 0$ (left) and $t = 48$ h (right) are respectively shown. A trough (P_0 at $t = 0$) moved to the point P during the 48 h numerical integration. A cross mark Q indicates an analytically exact position of the trough at $t = 48$ h.

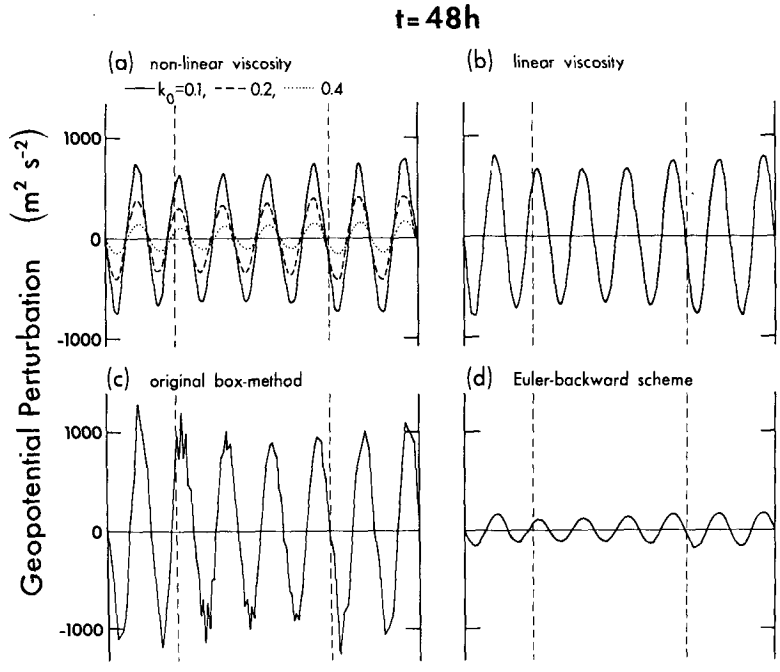

FIG. 7. Integrations of a train of 600 km waves with (a) nonlinear viscosity and (b) linear viscosity. Results of integration without vicosity by (c) the original box method and (d) the Euler-backward scheme are also shown. Dashed lines denote the mesh boundary.

due to the new method is clearly seen. Another feature of the integration is the use of the time integration scheme proposed by Kurihara and Tripoli (1976) which is designed to preserve low-frequency waves. If the integration is made with the Euler-backward scheme (e.g., Kurihara, 1965), the slowly moving wave is gradually suppressed to yield the field as shown in Fig. 7d at 48 h. Viscosity terms are not included in the integrations for Figs. 7c and 7d.

In a nested-mesh system, numerical behavior of a wave in one mesh domain is different from that in other domains. However, this did not cause any serious computational problem in the present tests provided the wave was resolved in the CM domain by six or more grid points. If the scale of a wave is reduced further, irregularities in the predicted fields become noticeable, especially in the FM domain. There, very short waves, unresolvable in the CM, are reflected off the interface and trapped. Such a difficult situation will develop inevitably in a nonlinear system, and it has to be kept under control. In Fig. 8a, a wave train with a wavelength of 300 km is shown. Time integration for this case was performed with the proposed scheme first without viscosity terms. The geopotential field after 48 h of integration is displayed in Fig. 8b, showing the development of noise. While the growth of noise is very sensitive to the finite difference scheme chosen to integrate the model, the noise is not excessively large in the present case. Next, an attempt is made to suppress the noise with nonlinear viscosity. This viscosity may also damp short waves which cannot be treated accurately in the CM anyway. Results of the 48 h integration which includes the diffusion are presented in Fig. 8c. With the parameter $k_0 = 0.4$, the wave train is almost entirely diffused. Fig. 8d shows the results after 48 h using the Euler-backward method. Presumably, this integration suppresses all waves except for standing waves. The figure indicates that a noise of a form of a standing mode remains if no viscosity term is included; such noise can be smoothed out by means of nonlinear viscosity.

b. Test of mesh movement

In this subsection, tests are made on the movement of a single disturbance which is superposed on a stationary field and which moves along a one-dimensional channel. The initial perturbation of the geopotential field consists of a disturbance ϕ' and a stationary component, ϕ_*, i.e.,

$$\phi = \phi' + \phi_* \tag{4.4}$$

The channel is 9600 km long and cyclic. The disturbance is specified by

$$\phi' = -S_0 \exp[-(x - x_0)^2/L^2] + C' \tag{4.5}$$

which applies for $|x - x_0| \leq 4800$ km and is re-

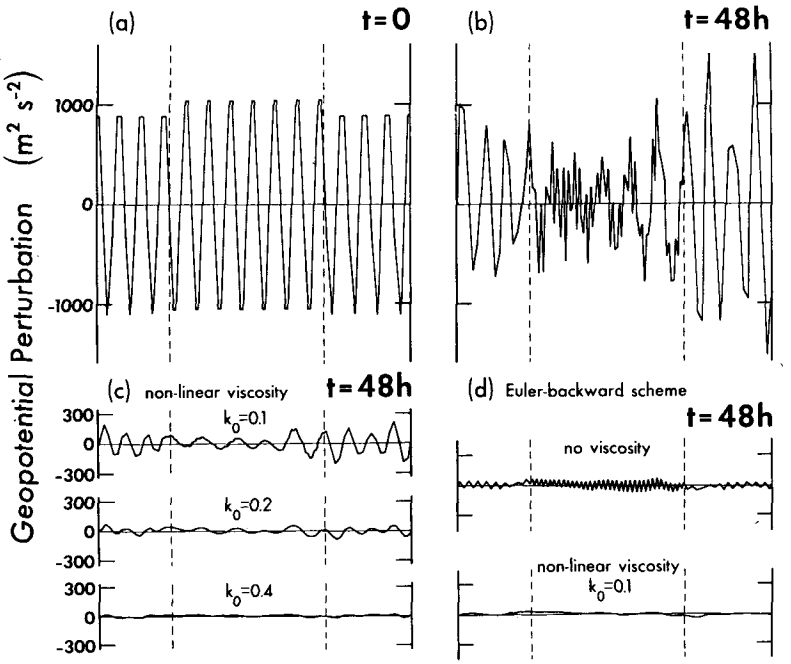

FIG. 8. Integration of a train of 300 km waves. Geopotential fields are shown at (a) $t = 0$, (b) $t = 48$ h, obtained without viscosity, (c) $t = 48$ h, with viscosity and (d) $t = 48$ h, computed by the Euler-backward scheme. Dashed lines denote mesh boundary.

peated in a cyclic manner. The scale of the disturbance is determined by L. In (4.5), C' is chosen so that the average of ϕ' in the channel vanishes. In this study, a disturbance with $S_0 = 1000$ m^{2}s^{-2} and $L = 173$ km is placed at $x_0 = 2010$ km. The stationary field is given by

$$\phi_* = -S_* \sin[(2\pi/D)x]. \tag{4.6}$$

The values for S_* and D will be specified later. The initial flow is assumed to be geostrophic: $u = 0$, $v = (\partial\phi/\partial x)/f$. The disturbance thus specified at the initial time will simply be advected in the channel if the fields are governed by

$$\left.\begin{aligned}
\frac{\partial u}{\partial t} &= -U\frac{\partial u}{\partial x} + fv - \frac{\partial \phi}{\partial x} \\
\frac{\partial v}{\partial t} &= -U\frac{\partial v}{\partial x} - fu + U\frac{\partial}{\partial x}\left(\frac{1}{f}\frac{\partial \phi_*}{\partial x}\right) \\
\frac{\partial \phi}{\partial t} &= -U\frac{\partial \phi}{\partial x} - gH\frac{\partial u}{\partial x} + U\frac{\partial \phi_*}{\partial x}
\end{aligned}\right\}. \tag{4.7}$$

The last terms in the above equations for v and ϕ are the forcing terms used to maintain the stationary field. Note that frictional effects are not included in (4.7). Numerical integration of (4.7) may reveal troublesome problems such as numerical dispersion of a pattern and generation of computational noise.

First, the case without a stationary field, i.e., $S_* = 0$ in (4.6), is considered. Numerical values in (4.7) are set to $U = 50$ m s^{-1}, gH $= 8 \times 10^4$ m^{2}s^{-2} and f is defined at 45° latitude. The results of a numerical integration at 0, 12, 24 and 36 h from a model with a uniform 60 km mesh and a 120 s time step are presented in the right part of Fig. 9. The phenomenon of numerical dispersion is clearly shown. An increase in the grid resolution near the disturbance will reduce the dispersion because small-scale components in the disturbance will be advected more accurately. The numerical results from a model in which a mesh of 20 km grid resolution is nested are shown in the middle part of Fig. 9. The integration for the inner domain is made with a 40 s time step. The fine grid domain is moved so that the grid point nearest to the position of the geopotential minimum always coincides with the center of the FM domain. Improvement of the result is considerable. When the grid distance in the fine mesh is reduced further to 10 km and the time step is reduced to 20 s, the disturbance moves without leaving a noticeable trailing irregularity. The results for this case are presented in the left part of the figure.

In the experiments mentioned above, the background field near the mesh interfaces remains flat

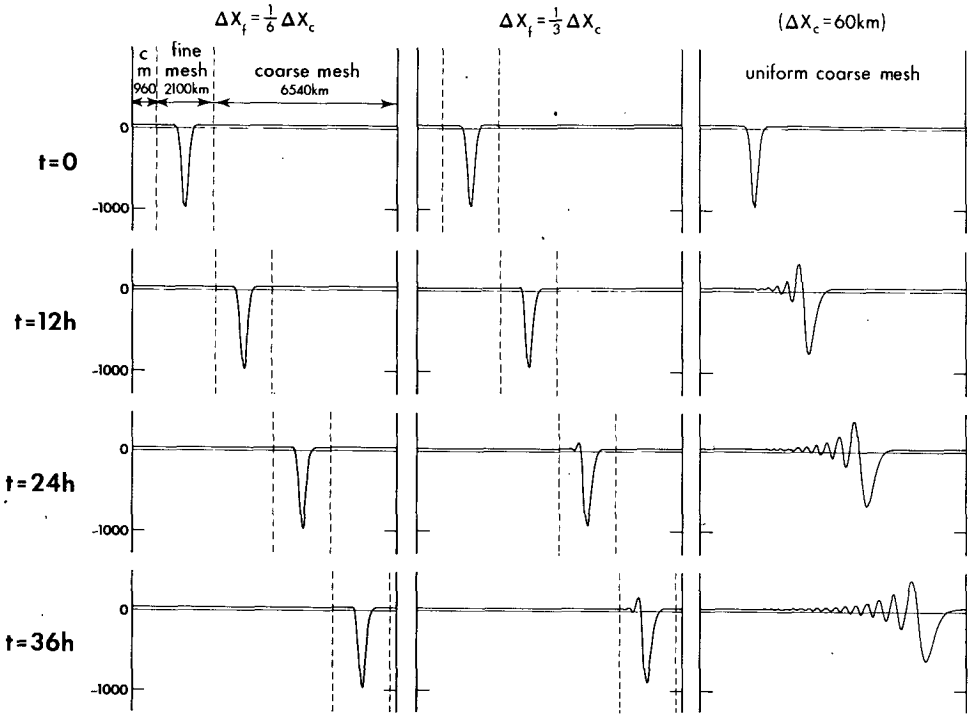

FIG. 9. Movement of a single disturbance in a one-dimensional cyclic free-surface channel. Integration is made with a moving nested mesh of 1:6 grid ratio (left), a moving nested mesh of 1:3 grid ratio (middle) and a uniform mesh of 60 km resolution (right). Geopotential perturbations are shown at $t = 0$, 12, 24 and 36 h. (from top to bottom)

over the 36 h period (see the fields near dashed lines in Fig. 9). In the following experiments, a stationary field is assumed so that a mesh interface moves on a spatially varying field. The stationary field is specified by Eq. (4.6). Numerical values in (4.6) are chosen as $S_* = 500$ m^{2}s^{-2} and $D = 9600$ km in one experiment and as $S_* = 500$ m^{2}s^{-2} and $D = 3200$ km in the other. A geostrophic disturbance, which takes the same shape as that in the previous experiments, is superposed on these stationary fields and the numerical integrations of (4.7) are performed. The mesh system used in these integrations is the one which yielded the left part of Fig. 9. The results of numerical integrations for the two cases are presented in Fig. 10. No noticeable noise is observed despite the fact that new grid data near the mesh interface were computed by the rather simple scheme as described before whenever the nested mesh moved.

5. Summary and remarks

In this paper, a design of a two-way nested-mesh system was described. This design features the separation of a dynamical interface from a mesh interface and the conservation of mass, momentum and internal energy. The proposed scheme was tested with a one-dimensional wave train model. When a wave is resolved sufficiently well by the coarse mesh, little noise is excited. However, shorter waves may cause irregularities, some of which are stationary, in the predicted field. In the present experiments, such noise could be controlled by diffusion.

The movement of the nested mesh requires resolution changes from coarse to fine at the leading edge of the mesh and vice versa at the trailing edge. An interpolation scheme to establish the data in the affected areas was proposed. The conservation of mass, momentum and internal energy is maintained during this movement. This scheme was tested by tracking a moving disturbance with a fine mesh. Although the experiments in the last section gave satisfactory results, there may be cases in which special caution and treatment are required to suppress noise. This is because a dynamical balance is not guaranteed between the mass and wind fields established by the mesh movement procedure.

In this paper, the numerical results from a one-dimensional two-way nested model are presented. Since the test experiments with this model were completed, an effort has been made to construct a three-dimensional movable nested-mesh model. The numerical formulation of the model is based entirely on the computation schemes described in this paper. Numerical experiments with the three-dimensional model are yielding very satisfactory results which will be reported in the future. In short, the proposed

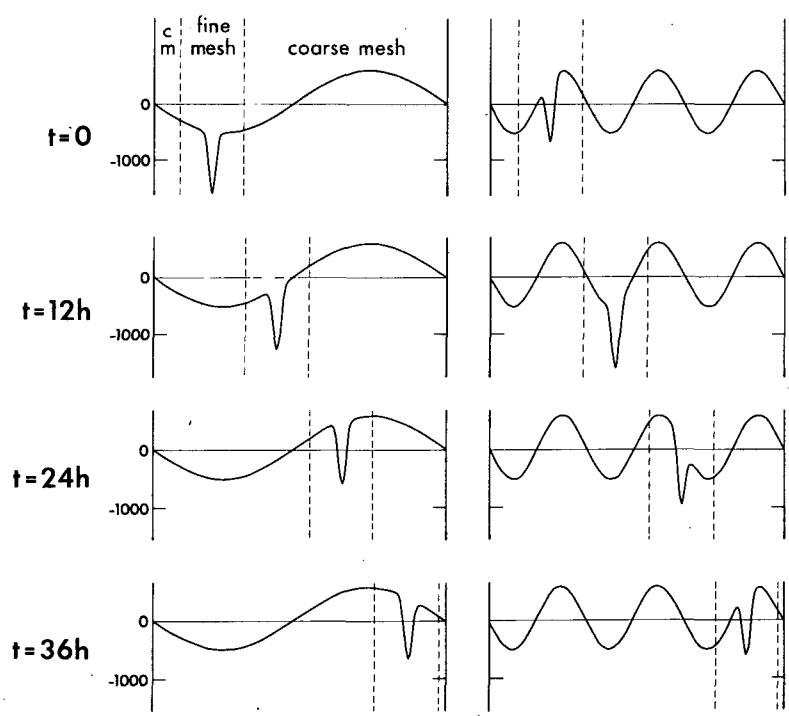

FIG. 10. As in Fig. 9 except that there exists a stationary field of 9600 km wavelength (left) and 3200 km wavelength (right). Integration is made with a moving nested mesh of 1:6 grid ratio.

mesh nesting strategy works equally well in a three-dimensional model as in a one-dimensional model. This fact prompted the present authors to publish this paper.

Acknowledgments. The authors thank J. Smagorinsky for encouragement throughout this study. They are grateful to W. R. Cotton, K. Miyakoda, B. B. Ross and R. E. Tuleya for the valuable comments on the original manuscript. They also express gratitude to Mrs. B. M. Williams and Messrs. J. N. Conner and P. G. Tunison for their assistance in the preparation of this manuscript.

REFERENCES

Harrison, E. J., and R. L. Elsberry, 1972: A method for incorporating nested finite grids in the solution of systems of geophysical equations. *J. Atmos. Sci.*, **29**, 1235–1245.

Kurihara, Y., 1965: On the use of implicit and iterative methods for the time integration of the wave equation. *Mon. Wea. Rev.*, **93**, 33–46.

——, and J. L. Holloway, 1967: Numerical integration of a nine-level global primitive equations model formulated by the box method. *Mon. Wea. Rev.*, **95**, 509–530.

——, and G. J. Tripoli, 1976: An iterative time integration scheme designed to preserve a low-frequency wave. *Mon. Wea. Rev.*, **104**, 761–764.

Ley, G. W., and R. L. Elsberry, 1976: Forecasts of typhoon Irma using a nested-grid model. *Mon. Wea. Rev.*, **104**, 1154–1161.

Miyakoda, K., and A. Rosati, 1977: One-way nested grid models: the interface conditions and the numerical accuracy. *Mon. Wea. Rev.*, **105**, 1092–1107.

Ookochi, Y., 1972: A computational scheme for the nesting fine mesh in the primitive equation model. *J. Meteor. Soc. Japan.*, **50**, 37–47.

Phillips, N. A., 1957: A coordinate system having some special advantages for numerical forecasting. *J. Meteor.*, **14**, 184–185.

——, and J. Shukla, 1973: On the strategy of combining coarse and fine grid meshes in numerical weather prediction. *J. Appl. Meteor.*, **12**, 763–770.